International Journal of Pharmaceutics 415 (2011) 293–300

Contents lists available at ScienceDirect

International Journal of Pharmaceutics

journal homepage: www.elsevier.com/locate/ijpharm

Pharmaceutical Nanotechnology

Preparation and antitumor study of camptothecin nanocrystals

Hua Zhang[a], Christin P. Hollis[b], Qiang Zhang[a,*], Tonglei Li[b,**]

[a] Department of Pharmaceutics, School of Pharmaceutical Sciences, Peking University, Beijing, 100191, China
[b] Department of Pharmaceutical Sciences, College of Pharmacy, University of Kentucky, Lexington, KY 40536, USA

ARTICLE INFO

Article history:
Received 19 December 2010
Received in revised form 23 April 2011
Accepted 28 May 2011
Available online 14 June 2011

Keywords:
Camptothecin
Nanocrystals
Nanosuspension
MCF-7
Antitumor efficacy

ABSTRACT

Camptothecin (CPT) is a potent, broad spectrum antitumor agent that inhibits the activity of DNA topoisomerase I. Due to its poor solubility and stability and consequent delivery challenges, its clinical use is nevertheless limited. We aim to use nanocrystal formulation as a way to circumvent the difficult solubilization practice. Specifically, camptothecin nanocrystals were prepared with a sonication–precipitation method without additional stabilizing surfactants. Particle characteristics, cellular cytotoxicity, and animal antitumor effect were examined. CPT nanocrystals were tested to be more potent to MCF-7 cells than CPT solution *in vitro*. When tested in MCF-7 xenografted BALB/c mice, the CPT nanocrystals exhibited significant suppression of tumor growth. The drug concentration in the tumor was five times more at 24 h by using the nanocrystal treatment than by using the drug salt solution. Storage stability study indicated that the nanocrystals were stable for at least six months. Overall, CPT nanocrystals were considered to be potentially feasible to overcome formulation challenges for drug delivery and to be used in clinic.

1. Introduction

Camptothecin (CPT) is a natural alkaloid found in the bark of *Camptotheca acuminata* (Wall et al., 1966). Despite numerous studies showing CPT as a promising antitumor compound, early clinical trials were abandoned because of its poor solubility (*ca.* 1.2 μg/mL) and unexpected toxicity (Potmesil, 1994; Venditto and Simanek, 2010). In the late 1980s when its pharmacological target was identified, CPT and its analogs have regained considerable interest as a cancer treatment regimen. It is found that CPT is able to inhibit DNA topoisomerase I (TOP I) through chemical binding between the enzyme and the acyl position of the CPT lactone ring (Hertzberg et al., 1989). The inhibition activity of CPT apparently relies on the presence of its lactone ring. Unfortunately, the pH-dependent hydrolysis of CPT lactone form leads to the opening of the lactone ring and becoming the inactive carboxylate form (Selvi et al., 2008). The degradation is further hastened by preferred affinity to human serum albumin (HSA) by the inactive, ring-opened form (Gabr et al., 1997; Burke and Mi, 1993). Still, lacking in better delivery means, CPT is commonly given as a sodium salt of the carboxylate form in clinic to overcome the poor solubility of the lactone form; this requires higher dose, which may lead to additional toxic reactions.

Given the undesired solubility and stability problems, a series of CPT analogues have been synthesized and a few have entered to the clinic (Venditto and Simanek, 2010). At the same time, various CPT delivery systems have been investigated, including micelles (Opanasopit et al., 2004; Kawano et al., 2006; Barreio-Iglesias et al., 2004; Fan et al., 2010), liposomes (Cortesi et al., 1997; Saetern et al., 2004), polymer conjugations (Yu et al., 2005; Hong et al., 2010), chitosan complexation (Zhou et al., 2010), and nanoparticles (Yang et al., 1999; Miura et al., 2004; Kunii et al., 2007). There are drawbacks, however, of many of these systems, such as low drug loading (Torchilin, 2007), poor physical stability and drug leakage (Mayer et al., 2000), and usage of solubilizing and/or encapsulating excipients that not only limit drug loading but may also impose adverse side effects. A recent report by Zhao et al. (2010a) shows that micronized CPT was prepared by a supercritical antisolvent (SAS) method, where DMSO was used as the solvent and CO_2 was used the antisolvent. The micronized CPT particles were characterized by a variety of analytical techniques, including SEM, AFM, XRD, FTIR, and DSC. The results suggested that the micronized CPT had a low level of crystallinity; the quasi-amorphous particles showed an enhanced solubility at about 30 μg/mL. The stability and *in vivo* effect, however, were not studied in their report. Clearly, low drug loading of many current CPT delivery systems

* Corresponding author at: Room 408, Pharmacy Building, Peking University, 38 Xueyuan Road, Beijing 100191, China. Tel.: +86 10 82802791; fax: +86 10 82802791.
** Corresponding author at: Room 375, Biological/Pharmaceutical Complex, University of Kentucky, 789 South Limestone Street, Lexington, KY 40536-0596, USA. Tel.: +1 859 257 1472; fax: +1 859 257 7585.
E-mail addresses: zqdodo@bjmu.edu.cn (Q. Zhang), tonglei@uky.edu (T. Li).

0378-5173/$ – see front matter © 2011 Elsevier B.V. All rights reserved.
doi:10.1016/j.ijpharm.2011.05.075

is inefficient for chemotherapy and poor chemical/physical stability, which, in some cases, is caused by the amorphous nature of the drug in the formulation, may further degenerate the treatment efficacy.

There has been an increased interest in formulating poorly soluble drugs into nanosized crystalline particles, in particular, for delivering anticancer drugs (Liu et al., 2010; Merisko-Liversidge et al., 2003). Several drug nanocrystal formulations have already made into the market, mainly as oral formulations (Rabinow, 2004). Apparently, being the most physically stable, nanocrystals require no solubilizing chemicals and thus offer high drug loading and much increased drug tolerance (Merisko-Liversidge et al., 2003). Herein, we report a nanocrystal formulation of CPT and its *in vitro* and *in vivo* performance against cancer.

2. Materials and methods

2.1. Materials

Camptothecin (purity > 99%) was purchased from 21CEC PHARM (London, United Kingdom). Dimethyl sulfoxide (DMSO, ACS grade) and acetonitrile (HPLC grade) are products of Fisher Scientific (Pittsburgh, PA, USA). Pluronic F127 and polyvinylpyrrolidone (PVP) K30 were obtained from BASF (Florham Park, NJ, USA) and Fluka Chemical (Steinheim, Switzerland), respectively. Hydroxypropyl methylcellulose (HPMC, K4M grade) was from Dow Chemical Company (Midland, MI, USA), and polyethylene glycol (PEG) 8000 and chlorpromazine from Sigma (St. Louis, MO, USA). Sulforhodamine B (SRB) was obtained from MP Biomedicals (Solon, OH, USA). Cell culture products, unless mentioned otherwise, were purchased from Invitrogen (Carlsbad, CA, USA). The cell lines, except for the MCF-7 used in animal study, were purchased from ATCC (Manassas, VA, USA); MCF-7 used in animal study was a gift from Chinese Academy of Medical Science (Beijing, China). All other reagents utilized were of analytical grade and used without any further purification.

2.2. Preparation of CPT nanocrystals

2.2.1. Preparation method

CPT nanocrystals were prepared by anti-solvent precipitation augmented by sonication. In brief, 1 mL DMSO solution of 1 mg/mL CPT was injected into 10 mL of pH 4 water at room temperature under rapid stirring and intense sonication (by an FS20 sonication bath from Fisher Scientific Co.). Specifically, the stirring speed was set 500 rpm for 10 min, followed by 300 rpm for 30 min and 100 rpm for 30 min. Several polymers were tested for stabilizing the size of nanocrystals by being respectively added to the water before the introduction of DMSO solution. The final product was filtered by 50-nm polycarbonate membrane filter and the nanocrystals was washed with 5 mL of pH 4 water three times prior to being re-suspended in pH 4 water.

2.2.2. Particle size and zeta potential (ZP) analysis

The mean particle size (*z*-average) and the polydispersity index (PdI) were determined by dynamic light scattering (DLS) (Malvern Zeta Sizer, Malvern Instruments, UK). Before the DLS measurement, each of our samples was vortexed for 5 s to avoid particle settlement. A sample was generally diluted with pH 4 water and a suitable scattering intensity was identified for collecting final experimental values.

2.2.3. Crystal morphology

A scanning electron microscope (SEM) (Hitachi 4300, Schaumburg, IL) was used to image CPT nanocrystals. An SEM sample was generally prepared by re-filtering a nanocrystal suspension with 50 nm Whatman nucleopore polycarbonate membrane. The filtered product was then air-dried and stored in a dessicator before attaching the filter paper to an SEM sample holder. The sample was then sputter coated with a conductive layer of gold palladium (Au/Pd) for 1 min, resulting in approximately 15 nm thick coating.

2.2.4. GC analysis of residual DMSO

The residual DMSO in CPT nanocrystals samples was analyzed by gas chromatography (GC). The system was an Agilent 7820A with a capillary column and a flame ionization detector (Agilent Technologies, USA). 40 mg of CPT nanocrystals were accurately weighed and dissolved with 10 mL *N*,*N*-dimethylformamide (DMF, analytical grade). 1.0 μL of the solution was injected into the GC system at a flow rate of 2.5 mL/min with nitrogen as the carrier gas. Oven temperature was maintained at 100 °C; the injector and detector temperature were set to 220 and 250 °C, respectively.

2.3. High-performance liquid chromatographic (HPLC) analysis of CPT

CPT concentrations in solution were detected by an HPLC system (Waters Breeze with a dual wavelength absorbance detector, Waters 2487, and multi λ fluorescence detector, Waters 2475). A reverse-phase C-18 column (5 μm, 150 mm × 4.6 mm, Waters) was used. The mobile phase was composed of 36% acetonitrile and 64% water, whose pH was adjusted to 5 with acetic acid. The column was eluted at a flow rate of 0.5 mL/min at 33 °C. The UV detector was used at 256 nm for measuring dissolution kinetics and stability of CPT nanocrystals and the fluorescence detector was used (λ_{ex}: 370 nm and λ_{em}: 435 nm) for measuring cellular uptake of the nanocrystals.

To measure the drug biodistribution, an aliquot of plasma or homogenized tumor or organ sample was acidified with hydrochloric acid (3 M), followed by CPT extraction by cold acetonitrile. The liquid mixture was vortexed for 1 min and centrifuged at 10,000 rpm for 10 min; 20 μL of the supernatant was injected at a flow rate of 1.0 mL/min into a Shimadzu HPLC system equipped with a fluorescence detector (λ_{ex}: 375 nm and λ_{em}: 435 nm) and a reverse-phase C-18 column (5 μm, 250 mm × 4.6 mm, Agilent). The mobile phase was composed of 35% acetonitrile and 65% acetic acid (0.1%). Calibration curves were established respectively for the tumor, organs and plasma; all of the correlation coefficients were more than 0.99.

2.4. In vitro dissolution of CPT nanocrystals

To measure dissolution kinetics, CTP nanocrystals were diluted by phosphate buffered saline (PBS; pH 7.2) to 30 μg/mL. 1 mL of the suspension was put in a dialysis tube (6000–8000 molecular weight cut-off, Fisherbrand®, Pittsburgh, PA, USA) that was then immerged in 200 mL of PBS at 37 °C and under constant shaking. 1 mL of the medium outside the dialysis tube was withdrawn at predetermined intervals for HPLC analysis of CPT concentration. For comparison, CPT dissolved in DMSO and further diluted in PBS was also tested by the same procedure. All experiments were performed in triplicate.

2.5. Storage stability study

The suspensions of CPT nanocrystals were stored at 4 °C or room temperature. Particle size, zeta potential, and polydispersity index of the samples were measured at 0, 1, 2, 3 and 6 months. Particle morphology was also monitored by SEM. In addition, the ring open reaction and concentration of CPT carboxylate form were detected by HPLC as well.

2.6. In vitro cytotoxicity of CPT nanocrystals

The *in vitro* cytotoxicity of CPT nanocrystals and DMSO solution were tested in human breast cancer cell MCF-7 and lung cancer cell A549. Cells were cultured in Dulbecco's Modified Eagle Medium (DMEM) medium supplemented with 10% fetal bovine serum (FBS) in a humidified atmosphere containing 5% CO_2 at 37 °C. The cells were seeded in a 96-well plate at a density of 0.6×10^4/well for MCF-7 or 0.4×10^4/well for A549. Nanocrystals were suspended in DMEM to 1 μg/mL and were further diluted from 1 to 1000 ng/mL for measurement. CPT DMSO solutions were also diluted in DMEM at the same concentration values. Cells were then exposed to a solution at 37 °C for 72 h and subjected to SRB assay. The optical densities were measured by a microplate reader (ELX 800, Bio-TEK Inc., USA) at 561 nm.

2.7. The cellular uptake of CPT nanocrystals

Cancer cells of MCF-7, A549, MDA-MB-231 or KB were seeded into a 24-well plate at a density of 1×10^4 cells/well and incubated at 37 °C. When cells approached 80% confluent, 20 μg/mL CPT solution or nanocrystals in DMEM were added and incubated for 30 min at 37 °C. The medium was then removed and cells were washed with cold PBS three times. 1 mL DMSO was added to each well, and the solution was collected, homogenized for 10 min, and centrifuged at 13,000 rpm for 10 min. 20 μL of the supernatant was injected to HPLC system for CPT quantification. As a competitive test, 20 μg/mL chlorpromazine was concurrently added to wells with CPT.

2.8. In vivo antitumor measurement

2.8.1. Formulation

As positive control, 150 mg CPT was dissolved in a mixture of 15 mL 1 M NaOH and 6 mL propylene glycol at 60 °C. Once CPT was dissolved, 25 mL water was added to the mixture and pH was adjusted to 7 with 3 M HCl. The solution was sterilized by filtration. The final concentration after filtration was about 3 mg/mL. It was further diluted with 0.9% saline to 1.5 mg/mL (to achieve the IV dose of 7.5 mg/kg) prior to the animal test. CPT nanocrystals were also diluted with 0.9% saline to the same concentration for the animal study.

2.8.2. Animal model

BALB/c female mice (20 g) were obtained from Experimental Animal Center of Peking University (Beijing, China). All of the animal experiments comply with the principles of care and use of laboratory animals and were approved by the Institutional Animal Care and Use Committee of Peking University Health Science Center. 0.1 mL of MCF-7 cells (1×10^7/mL) was inoculated subcutaneously to each mouse at the right armpit. The MCF-7 bearing mice were randomly grouped (5 for control, 6 for CPT salt solution, and 6 for CPT nanocrystals) one week after the inoculation. Saline was used as negative control; the dose was 7.5 mg/kg for the CPT salt solution or the nanocrystals. At Day 8, 11, and 14 after the cells inoculation, 0.1 mL of a respective treatment was given intravenously to each animal via tail vein. Tumor size was monitored daily with a caliper in two dimensions (*length* and *width*); tumor volume was then estimated as $length \times (width)^2/2$. The body weight of the mice was also monitored daily as an index of systemic toxicity. The mice were euthanized on Day 21 and tumors were excised and weighed. Tumor inhibition rate (IR) was calculated by:

$$\mathrm{IR} = \frac{W_{\mathrm{control}} - W_{\mathrm{treated}}}{W_{\mathrm{control}}}$$

Here W_{control} were the tumor weights of mice treated by saline and W_{treated} were the tumor weights of mice treated by the CPT salt solution and nanocrystals, respectively.

To determine the biodistribution of the drug, the above tumor-bearing animal model was also used. The CPT nanocrystals and CPT salt solution were intravenously administered to the mice (6 per group) via tail veins, respectively, at a dose of 7.5 mg/kg when the tumor volume reached approximately 100 mm^3. Blood was collected into heparinized test tubes and centrifuged to obtain the plasma at 0.5 h and 24 h after the treatment injection. The animals were then euthanized; organs and tumor samples were excised, washed with saline, weighed, and stored at −20 °C for further analysis.

2.9. Statistical analysis

For the cellular and animal studies, unpaired *t*-tests were performed for comparing the statistical difference among the treatments. For *p*-values that were 0.05 or less, the difference was considered significant.

3. Results and discussion

3.1. Nanocrystal preparation

CPT nanocrystals show rod- or needle-like morphology (Fig. 1) and the size ranges from 200 to 700 nm. To produce uniform, nanosized crystal particles within a narrow size distribution, the nucleation plays a crucial role. Sonication proved to be important for reducing particle size (data not shown). Ultrasound waves have been shown capable of enhancing nucleation by creating acoustic cavitation in solution and subsequently reducing the induction time (Guo et al., 2005; Kaerger and Price, 2004; Hem, 1967). Furthermore, the degree of supersaturation induced by the anti-solvent is also important in controlling the nucleation process. It is more desired that nucleation occurs swiftly so as to lead to crystals of similar sizes. As such, high supersaturation is needed and can be achieved by choosing a proper combination of good and anti-solvents. In our study, DMSO was the good solvent because CPT dissolves much more in DMSO (than other solvents, such as ethanol or acetone). In addition, pH 4 water was specifically selected as the anti-solvent system and the storage medium due to the fact that the lactone form of CPT predominantly exists when pH is less than 5 (Fassberg and Stella, 1992). These crystallization conditions were identified after numerous tests of various combinations of the controlled factors. Using high speed stirring and intense sonication was aimed to create a large number of nuclei simultaneously, crucial for producing nanosized and uniform crystal. Continuing growth was sustained by low speed stirring without sonication.

Long-chain polymeric surfactants may improve the physical stability of nanocrystals by reducing Ostwald's ripening (Rabinow, 2004; Van Eerdenbrugh et al., 2008; Zhao et al., 2010b). When various stabilizers were respectively introduced to the crystallization milieu, the shape and size of the nanocrystals were altered (Fig. 1B–E). Surprisingly, using the polymers resulted in the increased size of nanocrystals. The absolute values of zeta potential were decreased, on the other hand, because of the addition of the polymers. Typical CPT nanocrystal batch had a zeta potential of approximately −40 mV. However, when HPMC, PEG 8000, Pluronic F-F127, or PVP was incorporated in the process, their zeta potential values were changed to −22.9, −26.7, −19.5, and −13.9 mV, respectively. It seems that these polymers significantly reduced the electrostatic repulsion either through surface adsorption to the nanocrystals and/or affecting the dielectric constant of the liquid environment, not minimizing but augmenting the Ostwald's ripen-

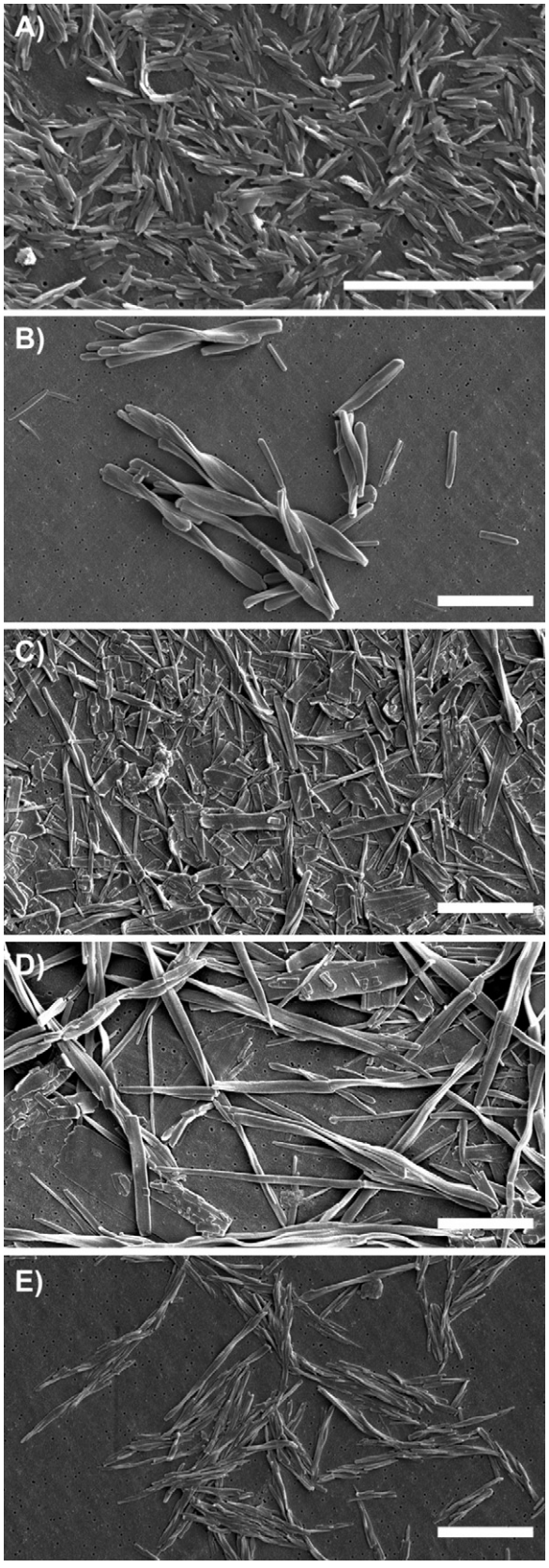

Fig. 1. SEM pictures of CPT nanocrystals grown without polymer additives (A) and with 0.25% (w/w) HPMC (B), 1% PEG 8000 (C), 1% Pluronic F-127 (D), and 0.5% PVP (E). Scale bar: 2.5 μm.

ing effect. As such, no polymer was used in preparing nanocrystals for *in vitro* and *in vivo* studies.

The residual DMSO in CPT nanocrystals was measured by GC (see Supplement Information) as 943 ppm, much smaller than the limit set by ICH of 5000 ppm for Class 3 solvents.

3.2. In vitro dissolution of CPT nanocrystals

Passage of CPT nanocrystals through the dialysis membrane was considerably delayed as compared with that of the CPT solution. 50% of nanocrystals were detected outside the dialysis membrane at 2 h while the time for the same amount of the CPT solution was 0.5 h. The results indicated that it took about 2 h for 15 μg CPT (half of the CPT in the dialysis tube) to dissolve. Note that this may be considered as sink condition because the eventual concentration when all CPT nanocrystals dissolved was much smaller than its solubility (*ca.* 1.2 μg/mL). Thus, conversely, it may take a much longer time for CPT nanocrystals to dissolve under a non-sink condition (e.g., in our *in vivo* study where 150 μg nanocrystals were given to a 20 g mouse that generally bears 2 mL plasma). Also note that the concentration shown in Fig. 2 includes those of both lactone and carboxylate forms. Nonetheless, the slow dissolution rate of CPT nanocrystals, due to its extremely low solubility, apparently adds to the benefit of delivering nanocrystals for chemotherapy in order to prolong the system circulation and maximize the enhanced permeability and retention (EPR) effect. EPR sets the cornerstone for targeted cancer drug delivery, as it is found that vasculatures in a tumor mass are much more "leaky" than those in healthy tissues and its lymphatic drainage is poorly developed, permitting the circulating drug carriers to enter the tumor and get trapped (Maeda, 2001). The solid particles may also curtail the hydrolysis of the drug, which must undergo in solution.

3.3. Storage stability

Suspensions of CPT nanocrystals were stored at 4 °C and room temperature, respectively. Particle size, polydispersity index (PdI), zeta potential, and CPT hydrolysis were monitored over six months (Table 1). Nanocrystals were also imaged by SEM (Supplement Information). Note that the particle size reported was determined by DLS, which approximates particle size by measuring diffusion coefficient and is more accurate in handling spherical particles. For high aspect-ratio particles, the method may still offer useful information particularly when keeping track of the same particle sample over time. Stored at the lower temperature, the particle size showed no significant change while the PdI was increased over the period of six months. Conversely, when stored at the room temperature, both size and PdI changed significantly. PdI obtained from the DLS measurement purports the width of a hypothetical, unimodal particle size distribution. The instrument calculated the PdI with the equation $(\sigma/Z_{avg})^2$, where σ and Z_{avg} are the size distribution and mean average size, respectively. As such, an increased PdI can be attributed to the widening of particle size distribution. Due to the Ostwald ripening phenomenon, small particles are dissolved and molecules are re-deposited to larger particles. At a lower temperature, although Ostwald ripening may be retarded, it is thought that the nanocrystal size was slowly evolving to two sets of distributions of smaller dissolving and larger growing particles. The average of particle size may still be close to the same average, but the PdI increased because the size distribution had been amplified. On the other hand, at ambient temperature, where Ostwald ripening was more facilitated, the re-deposition step to form larger particles became quicker, yielding larger particles. After six months, when the re-deposition step subsided, the PdI decreased suggesting the size distribution back to a unimodal model but of a larger size. Therefore, storage temperature clearly affected the stability of

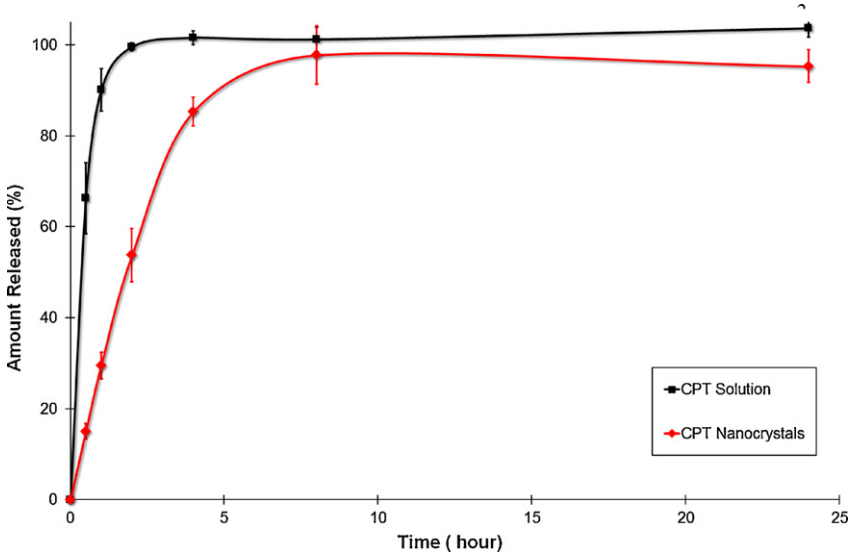

Fig. 2. *In vitro* releases profiles of CPT nanocrystals and solution in pH 7.4 phosphate buffer saline ($n = 3$).

Table 1
Particle properties of CPT nanocrystals stored at 4 °C and room temperature (RT).[a]

Duration (month)	Particle size (nm)		PdI		Zeta potential (mV)[b]		Carboxylate (%)[b]	
	4 °C	RT	4 °C	RT	4 °C	RT	4 °C	RT
0	234.4 ± 35.6	234.4 ± 35.6	0.134 ± 0.01	0.134 ± 0.01	−41.8 ± 1.3	−41.8 ± 1.3	0.0317 ± 0.0024	0.0317 ± 0.0024
1	244.8 ± 34.8	245.8 ± 33.3	0.140 ± 0.01	0.170 ± 0.03	−38.8 ± 2.0	−44.8 ± 1.4	0.0045 ± 0.0017	0.0587 ± 0.0011
2	241.9 ± 37.2	264.7 ± 58.2	0.151 ± 0.01	0.199 ± 0.05	−34.6 ± 2.6	−43.3 ± 2.4	0.0036 ± 0.0006	0.0630 ± 0.0028
3	243.6 ± 37.1	246.8 ± 36.2	0.163 ± 0.02	0.192 ± 0.01	−27.7 ± 3.4	−46.5 ± 2.0	0.0030 ± 0.0010	0.1570 ± 0.0240
6	241.4 ± 31.3	438.5 ± 180.8	0.162 ± 0.02	0.125 ± 0.08	N/A	N/A	N/A	N/A

[a] Each measurement was done in triplicate.
[b] Zeta potential and the amount of CPT carboxylate form were only monitored for 3 months because of insufficient amount of samples for analysis.

the nanocrystals; at low temperature, the stability of nanocrystals can at least be maintained for six months. Despite some uncertainly in particle size measurement by DLS that was due to the large aspect ratio of nanocrystals, the change in particle size and morphology revealed by SEM imaged agreed with that by DLS. From the SEM images (Supplement Information), the size and morphology showed no significant change at 4 °C; some particles became slightly thicker after sixth months stored at room temperature. In either case, no aggregation was observed.

Interestingly, the absolute value of zeta potential of the nanocrystals decreased over the period of storage time at 4 °C, while it increased slightly when stored at the room temperature. This observation may be due to the temperature influence on the hydrolysis of the drug. Dissolution of the nanocrystals and the degradation were likely enhanced at the higher temperature and, as a result, more carboxylate forms were produced. As the ratio of carboxylate to lactone increased, the zeta potential might become more negative.

3.4. *In vitro* cytotoxicity of CPT nanocrystals

Cytotoxicity of CPT nanocrystals was evaluated in cancerous MCF-7 and A549 cell lines; CPT solution was tested as well for comparison. The half maximal inhibitory concentrations (IC_{50}) were determined from the concentration-dependent cell viability curves (Fig. 3). Of CPT nanocrystals, IC_{50} were 0.087 μM and 0.471 μM in MCF-7 and A549 cells, respectively; the corresponding values of the CPT solution were 0.129 μM and 0.507 μM. The difference was statistically significant ($p < 0.05$) between the nanocrystals and solution in MCF-7 cells, but not in A549. Additionally, it seems that CPT was more potent against MCF-7 cells. Note that in the cytotoxicity experiments, drug nanocrystals were incubated with cells for 72 h before the results were analyzed. As such, a majority of nanocrystals were likely dissolved in the medium, leading to similar cytotoxic performance to that of drug solution. The seemingly better (or more potent) cytotoxicity of the nanocrystals could also be resulted from the deterred hydrolysis of the drug molecules in the crystal. Furthermore, the results suggest that the IC_{50} values were

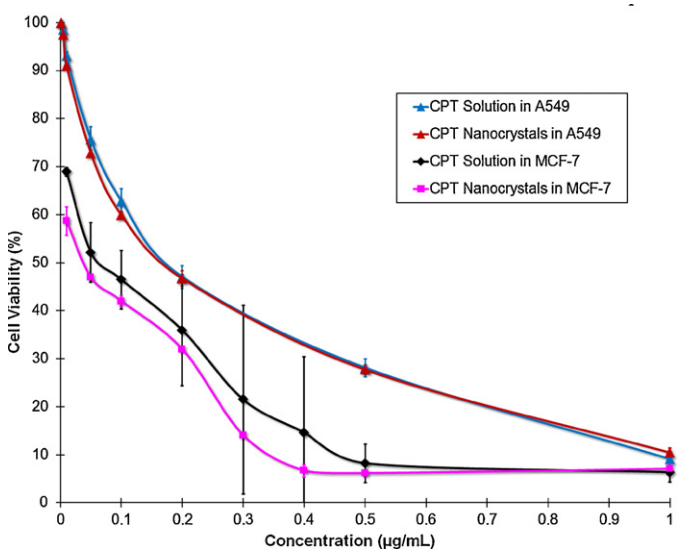

Fig. 3. *In vitro* cytotoxicity of CPT nanocrystals and solution against A549 and MCF-7 cells at 37 °C ($n = 3$).

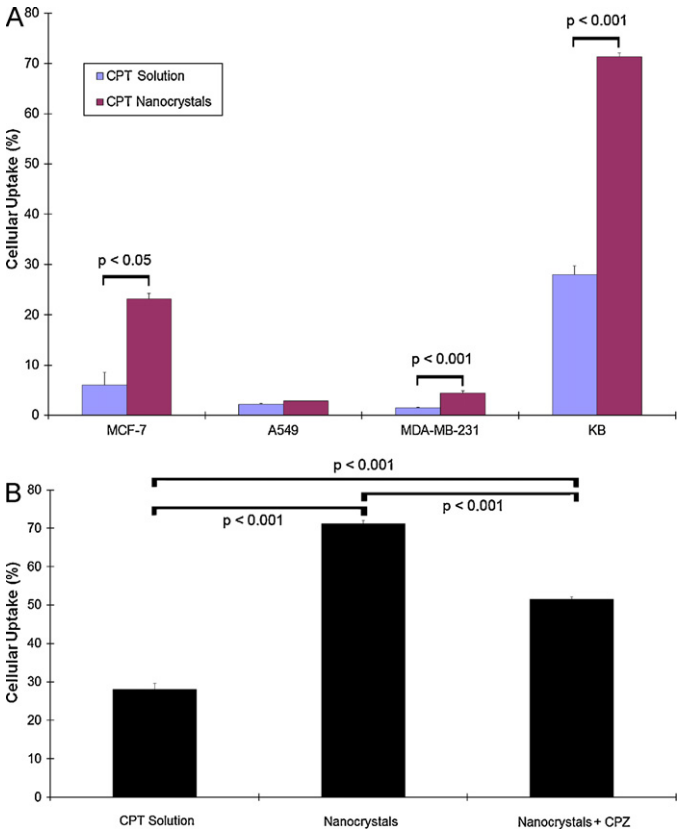

Fig. 4. Cellular uptake of CPT nanocrystals and solution in MCF-7, A549, MDA-MB-231 and KB cells exposed to the drug (A) and in KB cells exposed to the drug and chlorpromazine, CPZ (B) for 30 min at 37 °C ($n = 3$).

much smaller than the solubility of CPT (3.4 μM) thus making CPT nanocrystals feasible for being directly administered to treat cancers. Note that cell viability was not tested at low concentrations; this may skew the IC_{50} values to some extent.

3.5. Cellular uptake of CPT nanocrystals

Cellular uptake of CPT nanocrystals and solutions was characterized in MCF-7, A549, MDA-MB-231 and KB cell lines (Fig. 4A). The uptake ratios between the CPT nanocrystals and solution in MCF-7, A549, MDA-MB-231, and KB cell line were 3.87, 1.28, 2.93 and 2.54, respectively. Amongst the four cell lines studied, KB cells displayed the highest sensitivity to the CPT nanocrystals (of an uptake percentage of 71%), followed by MCF-7 (23%). Although the difference was more subtle, the same tendency was observed in MDA-MB-231. CPT nanocrystals were not as quite sensitive to A549 cells. Based on the cellular uptake results (Fig. 4A), it is believed that, in addition to passive diffusion of dissolved free molecules across the cell membrane, CPT nanocrystals, depending on their size, may be directly taken up by the cells via multiple endocytosis pathways, which may include clathrin-mediated, non-clathrin-mediated (e.g., caveolae), macropinocytosis, and phagocytosis. It is possible that particles with a size of 200 nm or smaller may be preferentially internalized via the clathrin-coated pits (Rejman et al., 2004; Zuhorn et al., 2002). To investigate whether this particular pathway was taking part in the internalization process, chlorpromazine (CPZ), which is known to disrupt clathrin and thereby clathrin-mediated endocytosis, was added to the cell media (Diaz-Moscoso et al., 2010). Because CPZ causes the loss of coated pits from the cell surface and their assembly around endosomal membrane, it prevents the recycling of clathrin to the plasma

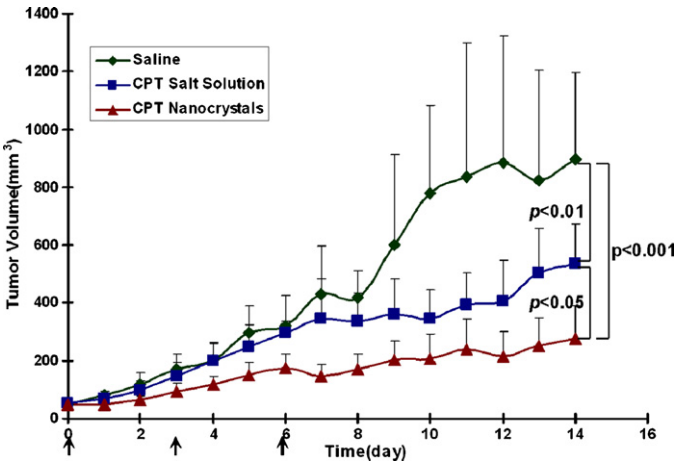

Fig. 5. Antitumor effect tested in MCF-7 bearing mice by saline ($n = 5$), CPT salt solution ($n = 6$), and CPT nanocrystals ($n = 6$). For each animal, three consecutive doses were given (marked by arrows).

membrane (Wang et al., 1993). In the presence of CPZ, the uptake of the CPT nanocrystals decreased significantly ($p < 0.001$ vs. CPT nanocrystals; Fig. 4B), suggesting that clathrin-assisted endocytosis contributes to the cellular uptake of the nanocrystals. Furthermore, the significant difference ($p < 0.001$) between the uptake of the CPZ-co-nanocrystals and CPT solution (Fig. 4B) indicates that nanocrystals were also taken up by additional endocytosis pathways. It is also possible that the CPZ dose was too low to completely inhibit the clathrin-assisted endocytosis. The internalization of nanocrystals with the size between 200 and 500 nm could be due to the caveolae-mediated pathway rather than clathrin-mediated (Rejman et al., 2004). To further unravel the cellular uptake mechanism, the *in vitro* examination was carried out at two different temperatures, 4 °C and 37 °C. It was found that there was a total uptake decrease of 265 or 301 ng for CPT solution or nanocrystals at 4 °C relative to that at 37 °C. Compared with the CPT solution, the larger decrease of the CPT nanocrystals uptake was not only due to the retardation in diffusion of single molecules across the cell membrane, but also resulted from deactivation of endocytosis of nanocrystals, which requires energy sources (e.g., ATP) and can thereby diminish at lower temperature. These results support the aforesaid claim that the nanocrystals are taken up by cells via active membrane transport process, likely the clathrin- and caveolae-mediated endocytosis.

3.6. In vivo antitumor effect of CPT nanocrystals

At the dose of 7.5 mg/kg, CPT nanocrystals (NCs) were consecutively administered to each MCF-7 bearing mouse via tail vein on Day 8, 11, and 14 after the tumor cell inoculation. CPT salt solution and saline were given to control groups in the same manner. The change in body weight (see Supplement Information) indicates that the mice experienced a slight weight loss only at the beginning of the treatment by the drug solution or nanocrystals. The weight loss was recovered in the following one or two days and there was no significance difference in body weight between the treatment groups, suggesting that the dose toxicity by the nanocrystals was acceptable. From the tumor progression results (Fig. 5), both treatment groups given by the nanocrystals and salt solution yielded significant tumor inhibition compared with the negative control group. The nanocrystal treatment was especially better than either the negative or the group treated by the salt solution; the statistical difference was significant ($p < 0.05$; Fig. 5). Calculated tumor inhibition rates based on the averaged weight of the tumors, which were dissected from the terminated animals, further indicate the better

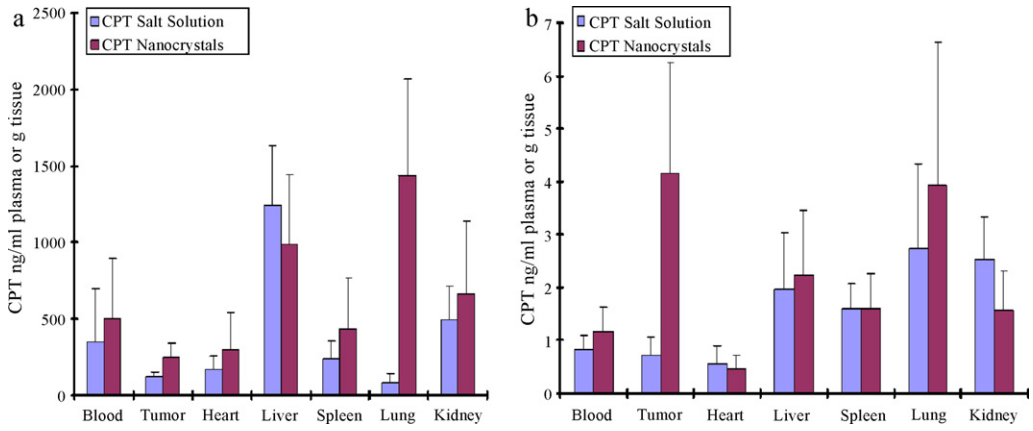

Fig. 6. CPT biodistribution in MCF-7-bearing mice after 0.5 h (a) and 24 h (b) treatment by drug salt solution and nanocrystals. Each bar represents the mean ± SE ($n = 6$).

therapeutic effect by the nanocrystals. In average, the tumor weight of the negative control (saline), treated with the salt solution, or CPT nanocrystals was 1.41, 0.67, or 0.51 g. Relative to the untreated group, the inhibition rates were 52% and 64% for the salt solution and nanocrystals, respectively, which were statistically different ($p < 0.001$). When observed either from the tumor progression chart (Fig. 5) or the final weight of the tumor, the nanocrystal formulation proved better efficacy. For the salt solution, upon tail vein injection, the molecules were directly in contact with blood, especially the serum albumin; thus, the lactone ring was quickly hydrolyzed to the ring open form of carboxylate, which is less potent (Burke and Mi, 1993). In contrast, drug molecules in the nanocrystals were slowly released and undissolved ones should maintain their active lactone form. In addition, the nanocrystals could also achieve prolonged circulation in the plasma. To that end, CPT nanocrystals were superior to the solubilized molecules and capable of targeting the tumor site via the EPR effect. At the cellular level, the drug could be transported either as free molecules by diffusion or as nanoparticles by active passage, considerably improving the antitumor activity.

3.7. CPT biodistribution in tumor-bearing mice

Biodistribution of CPT in the tumor, plasma, and major organs was examined after the treatment of CPT salt solution and CPT nanocrystals at a comparable dose of 7.5 mg/kg. Shown in Fig. 6, at 0.5 h subsequent to the injection, except in liver, the amount of CPT accumulation in the CPT nanocrystals treated group was higher than that treated by the salt solution. More interestingly, there was nearly twice as much total CPT concentration in the tumor when CPT nanocrystals were administered. At 24 h, the CPT accumulation in the tumor treated by the nanocrystals was significantly higher, by more than five folds, than that by the solution. Furthermore, the lactone percentages in the tumor were 81% and 36% by the nanocrystals and salt solution treatments, respectively. The high accumulation of the nanocrystals in the lung at the beginning of the treatment was suspected due to some relatively large nanocrystals.

The better treatment efficacy by using the drug nanocrystals was likely resulted from the larger accumulation in the tumor (Fig. 6) and the deterred hydrolysis of the drug. It is a common reception that nanoparticles should be made around 200 nm in order to take advantage of the EPR effect. Yet, our nanocrystals were much larger but still showed the preferred tumor accumulation compared with the solution formulation. One possible reason is that the pore size of the tumor vasculature was large than 200 nm. It is reported in the literature that the vascular pore cutoff of subcutaneously grown tumors, depending on the cell line, may vary from 200 nm to 1.2 μm (Hobbs et al., 1998). Another reason is that our nanocrystals were needle-like, with the shorter dimension being less than 50 nm. Gratton et al. reported that Hela cells can internalize non-spherical particles as large 3 μm via different endocytosis pathways and, more importantly, particles of high aspect ratio have higher internalization rate (Gratton et al., 2008).

4. Conclusions

In this study, camptothecin nanocrystals were prepared by an anti-solvent crystallization method augmented by ultrasonic wave. No surfactants were utilized. The obtained nanocrystals were needle-like and stable for at least six months stored in low temperature. Cytotoxicity and cellular uptake studies indicated that the drug nanocrystals could induce similar, if not better, cell growth inhibition compared with the solvated drug. The antitumor effect was significantly enhanced by the nanocrystals in treating tumor-bearing mice. The results suggest that it is not only possible to formulate nanocrystals of camptothecin, but also potentially feasible and favorable for clinical usage.

Acknowledgement

The authors acknowledge the financial support from DOD Idea Award Grant #: BC050287.

Appendix A. Supplementary data

Supplementary data associated with this article can be found, in the online version, at doi:10.1016/j.ijpharm.2011.05.075.

References

Barreio-Iglesias, R., Bromberg, L., Temchenko, M., Hatton, T.A., Concheiro, A., Alvarez-Lorenzo, C., 2004. Solubilization and stabilization of camptothecin in micellar solutions of pluronic-g-poly(acrylic acid) copolymers. J. Control. Release 97, 537–549.

Burke, T.G., Mi, Z., 1993. Preferential binding of the carboxylate form of camptothecin by human serum albumin. Anal. Biochem. 212, 285–287.

Cortesi, R., Esposito, E., Maietti, A., Menegatti, E., Nastruzzi, C., 1997. Formulation study for the antitumor drug camptothecin: liposomes, micellar solution, and a microemulsion. Int. J. Pharm. 159, 95–103.

Diaz-Moscoso, A., Vercauteren, D., Rejman, J., Benito, J.M., Mellet, C.O., De Smedt, S.C., Fernandez, J.M.G., 2010. Insights in cellular uptake mechanisms of pDNA-polycationic amphiphilic cyclodextrin nanoparticles (CDplexes). J. Control. Release 143, 318–325.

Fan, H.L., Huang, J., Li, Y.P., Yu, J.H., Chen, J.H., 2010. Fabrication of reduction-degradable micelle based on disulfide-linked graft copolymer–camptothecin conjugate for enhancing solubility and stability of camptothecin. Polymer 51, 5107–5114.

Fassberg, J., Stella, V.J., 1992. A kinetic and mechanistic study of the hydrolysis of camptothecin and some analogus. J. Pharm. Sci. 81, 676–684.

Gabr, A., Kuin, A., Aalders, M., El-Gawly, H., Smets, L.A., 1997. Cellular pharmacokinetics and cytotoxicity of camptothecin and topotecan at normal and acidic pH. Cancer Res. 57, 4811–4816.

Gratton, S.E.A., Ropp, P.A., Pohlhaus, P.D., Luff, J.C., Madden, V.J., Napier, M.E., Desimone, J.M., 2008. The effect of particles design on cellular internalization pathways. Proc. Natl. Acad. Sci. U.S.A. 105, 11613–11618.

Guo, Z., Zhang, M., Li, H., Wang, J., Kougoulos, E., 2005. Effect of ultrasound on anti-solvent crystallization process. J. Cryst. Growth 273, 555–563.

Hem, S.L., 1967. The effect of ultrasonic vibrations on crystallization processes. Ultrasonics 5, 202–207.

Hertzberg, R.P., Caranfa, M.J., Hecht, S.M., 1989. On the mechanism of topoisomerase I inhibition by camptothecin: evidence for binding to an enzyme–DNA complex. Biochemistry 28, 4629–4638.

Hobbs, S., Monsky, W.L., Yuan, F., Roberts, W.G., Griffith, L., Torchilin, V.P., Jain, R.K., 1998. Regulation of transport pathways in tumor vessels: role of tumor type and microenvironment. Proc. Natl. Acad. Sci. U.S.A. 95, 4607–4612.

Hong, M., Zhu, S., Jiang, Y., Tang, G.T., Sun, C., Fang, C., Shi, B., Pei, Y., 2010. Novel anti-tumor strategy: PEG–hydroxycamptothecin conjugate loaded transferring–PEG-nanoparticles. J. Control. Release 141, 22–29.

Kaerger, J.S., Price, R., 2004. Processing of spherical crystalline particles via a novel solution atomization and crystallization by sonication (SAXS) technique. Pharm. Res. 21, 372–381.

Kawano, K., Watanabe, M., Yamamoto, T., Yokoyama, M., Opanasopit, P., Okano, T., Maitani, Y., 2006. Enhance antitumor effect of camptothecin loaded in long-circulating polymeric micelles. J. Control. Release 112, 329–332.

Kunii, R., Onishi, H., Machida, Y., 2007. Preparation and antitumor characteristics of PLA/(PEG-PPG-PEG) nanoparticles loaded with camptothecin. Eur. J. Pharm. Biopharm. 67, 9–17.

Liu, F., Park, J., Zhang, Y., Conwell, C., Liu, Y., Bathula, S.R., Huang, L., 2010. Targeted cancer therapy with novel high drug-loading nanocrystals. J. Pharm. Sci. 99, 3542–3551.

Maeda, H., 2001. The enhanced permeability and retention (EPR) effect in tumor vasculature: the key role of tumor-selective macromolecular drug targeting. Adv. Enzyme Regul. 41, 189–207.

Mayer, L.D., Krishna, R., Webb, M., Bally, M., 2000. Designing liposomal anticancer drug formulations for specific therapeutic applications. J. Liposome Res. 10, 99–115.

Merisko-Liversidge, E., Liversidge, G.G., Cooper, E.R., 2003. Nanosizing: a formulation approach for poorly-water-soluble compounds. Eur. J. Pharm. Sci. 18, 113–120.

Miura, H., Onishi, H., Sasatsu, M., Machida, Y., 2004. Antitumor characteristics of methoxypolyethylene glycol-poly(DL-lactic acid) nanoparticles containing camptothecin. J. Control. Release 97, 101–113.

Opanasopit, P., Yokoyama, M., Watanabe, M., Kawano, K., Maitani, Y., Okano, T., 2004. Block copolymer design for camptothecin incorporation into polymeric micelles for passive tumor targeting. Pharm. Res. 21, 2001–2008.

Potmesil, M., 1994. Camptothecin: from bench research to hospital wards. Cancer Res. 54, 1431–1439.

Rabinow, B.E., 2004. Nanosuspensions in drug delivery. Nat. Rev. Drug Discov. 3, 785–796.

Saetern, A.M., Brandl, M., Bakkelund, W.H., Sveinbjornsson, B., 2004. Cytotoxic effects of different camptothecin formulations on human colon carcinoma in vitro. Anticancer Drugs 15, 899–906.

Rejman, J., Oberle, V., Zuhorn, I.S., Hoekstra, D., 2004. Size-dependent internalization of particles via the pathways of clathrin- and caveolae-mediated endocytosis. Biochem. J. 377, 156–169.

Selvi, B., Patel, S., Savva, M., 2008. Physicochemical characterization and membrane binding properties of camptothecin. J. Pharm. Sci. 97, 4379–4390.

Torchilin, V.P., 2007. Micellar nanocarriers: pharmaceutical perspectives. Pharm. Res. 24, 1–16.

Van Eerdenbrugh, B., Van den Mooter, G., Augustijns, P., 2008. Top-down production of drug nanocrystals: nanosuspension stabilization, miniaturization and transformation into solid products. Int. J. Pharm. 364, 64–75.

Venditto, V.J., Simanek, E.E., 2010. Cancer therapies utilizing the camptothecin: a review of *in vivo* literature. Mol. Pharm. 7, 307–314.

Wall, M.E., Wani, M.C., Cooke, C.E., Palmer, K.H., McPhail, A.T., Sim, G.A., 1966. Plant antitumor agents. I. The isolation and structure of camptothecin, a novel alkaloidal leukemia and tumor inhibitor from *Camptotheca acuminata*. J. Am. Chem. Soc. 88, 3888–3890.

Wang, L.H., Rothberg, K.G., Anderson, R.G., 1993. Mis-assembly of clathrin lattices on endosomes reveals a regulatory switch for coated pit formation. J. Cell Biol. 123, 1107–1117.

Yu, D., Peng, P., Dharap, S.S., Wang, Y., Mehlig, M., Chandna, P., Zhao, H., Filpula, D., Yang, K., Borowski, V., Borchard, G., Zhang, Z.H., Minko, T., 2005. Antitumor activity of poly(ethylene glycon)-camptothecin conjugate: the inhibition of tumor growth in vivo. J. Control. Release 110, 90–102.

Yang, S., Lu, L., Cai, Y., Zhu, J., Liang, B., Yang, C., 1999. Body distribution in mice of intravenously injected camptothecin solid lipid nanoparticles and targeting effect on brain. J. Control. Release 59, 299–307.

Zhao, X.H., Zu, Y.G., Li, Q.Y., Wang, M.X., Zu, B.S., Zhang, X.N., Jiang, R., Zu, C.L., 2010a. Preparation and characterization of camptothecin powder micronized by a supercritical antisolvent (SAS) process. J. Supercrit. Fluids 51, 412–419.

Zhao, Y., Hua, H., Chang, M., Liu, W., Zhao, Y., Liu, H., 2010b. Preparation and cytotoxic activity of hydroxycamptothecin nanosuspensions. Int. J. Pharm. 392, 64–71.

Zhou, L., Li, X., Chen, X., Li, Z., Liu, X., Zhou, S., Zhong, Q., Yi, T., Wei, Y., Zhao, X., Qian, Z., 2010. In vivo antitumor and antimetastatic activities of camptothecin encapsulated with N-trimethyl chitosan in a preclinical mouse model of liver cancer. Cancer Lett. 297, 56–64.

Zuhorn, I.S., Kalicharan, R., Hoekstra, D., 2002. Lipoplex-mediated transfection of mammalian cells occurs through the cholesterol-dependent clathrin-mediated pathway of endocytosis. J. Biol. Chem. 277, 18021–18028.